UNIVERSITY OF LEEDS

Article:
Anantharaman, SB, Messmer, D, Sadeghpour, A orcid.org/0000-0002-0475-7858 et al. (3 more authors) (2019) Excitonic channels from bio-inspired templated supramolecular assembly of J-aggregate nanowires. Nanoscale, 11 (14). pp. 6929-6938. ISSN 2040-3364

https://doi.org/10.1039/c8nr10357g

Excitonic Channels from Bio-Inspired Templated Supramolecular Assembly of J-aggregate Nanowires

Surendra B. Anantharaman,[1,2] Daniel Messmer,[3] Amin Sadeghpour,[4, 5, 6] Stefan Salentinig,[5] Frank Nüesch,[1,2] A. Dieter Schlüter,[3] Jakob Heier[1,*]

[1] Laboratory for Functional Polymers, Swiss Federal Laboratories for Materials Science and Technology (Empa), Überlandstrasse 129, CH-8600 Dübendorf, Switzerland.

[2] Institut des matériaux, École Polytechnique Fédérale de Lausanne (EPFL), CH-1015 Lausanne, Switzerland.

[3] Laboratory of Polymer Chemistry, Department of Materials, ETH Zurich, Vladimir-Prelog-Weg 5, 8093 Zürich, Switzerland.

[4] Center for X-ray Analytics, Swiss Federal Laboratories for Materials Science and Technology (Empa), Überlandstrasse 129, CH-8600 Dübendorf, Switzerland.

[5] Laboratory for Biointerfaces and [6] Laboratory for Biomimetic Membranes and Textiles , Swiss Federal Laboratories for Materials Science and Technology (Empa), Lerchenfeldstrasse 5, St. Gallen, CH-9014, Switzerland.

Corresponding Author

*Email: jakob.heier@empa.ch Phone: 041 58 765 4356

Abstract

Supramolecular assemblies such as J-aggregates with controlled growth of tubular morphology are of paramount importance for energy transport systems in organic semiconductors. Despite the synthetic freedom to design molecular structures of dyes that form J-aggregates, achieving 1-dimensional structures is highly limited. Here we demonstrate a simple and effective route to functionalize dendronized polymers (DPs) with J-aggregates to construct tubular J-aggregate/DP nanowires. When J-aggregates are adsorbed onto DPs anchored to glass substrates, they assemble into microcrystalline domains typically for J-aggregates adsorbed onto functionalized surfaces. Differently, a complexation between the dendronized polymer and J-aggregates in solution leads to dense packing of J-aggregate strands in the interior and on the outer surface of the DPs. Using a layer-by-layer (LBL) technique, these aggregates can be adsorbed onto a surface covered with a monolayer DP template. The thin film absorption spectra have a narrower FWHM and higher ratio of J-aggregate to monomer and dimer absorption than J-aggregates directly assembled onto a surface. This is a first time demonstration for a very promising approach to realize 1D light harvesting artificial antennas which can find application in opto-electronic devices.

1. Introduction

The realization of artificial systems with efficient exciton transport properties is of outermost relevance for the development of future optoelectronic devices. Naturally occurring photosynthetic light-harvesting systems, like chlorophyll molecules in a protein scaffold, act as antennas for exciton transport from the photosystem to the acceptor location within reach of 20-200 nm with a near-unity efficiency.[1, 2] Inspired by these antennae systems, self-assembling organic dye monomer molecules into supramolecular structures with higher-order organization such as J-aggregates, and edge-to-edge arrangement leads to strong transition dipole coupling. This unique coupling property causes collective optical (resonance energy transfer) properties and excitonic transport. Two dimensional brickstone structure J-aggregates, known for large coherent excited state domain sizes and

Förster resonance energy transfer (FRET) have shown exciton delocalization over more than 10000 molecules.[3] Recently, unprecedented exciton coherence in J-aggregates up to 1 μm was realized,[4] surpassing the exciton coherence length of chlorophyll systems of ~20-200 nm.[2] In parallel, several hybrid systems between quantum dots (QDs) and J-aggregates were developed to study the energy transfer from J-aggregates to QDs and vice versa. Walker et al.[5] have reported ~ 90% energy transfer efficiency from J-aggregates (donor) to QDs (acceptor) in a blend. Recently, Wang and Weiss[6] demonstrated J-aggregates as *"exciton-bridge"* between two lead sulfide QDs which act as donor and acceptor. The presence of J-aggregate bridges resulted in a 20-fold faster energy transfer rate than having the QDs closely linked by a polyelectrolyte. This functionality of the J-aggregate when integrated in energy harvesting systems can play a pivotal role in exciton transport for building efficient devices. Interestingly, the above mentioned studies were conducted with J-aggregates from a class of cyanine dyes with tubular morphology as exciton transport is superior along the tubular direction.[7, 8] Despite extensive research interest in tubular J-aggregates,[8-16] they are scarce and tuning the morphology of the J-aggregate is very challenging.[9, 17, 18] Limitations of the tubular J-aggregate morphology at different absorption edges is the bottleneck in realizing this technique in the field of exciton transport systems. Furthermore, they are poorly soluble and cannot be processed into thin films. Here tubular aggregates share a general short-coming of J-aggregates. Film formation properties are poor (when deposited from solution onto a substrate) or labor intensive (using LB techniques). Optical coherence properties in the thin film are typically worsening compared to solution.

Nature itself suggests an elegant solution: in light harvesting antennas, protein scaffolds assemble chromophores in a desired fashion. Similar approaches were followed by a number of research groups. Scaffolding of cyanine dye molecules on one-dimensional templates including DNA,[19, 20] viruses,[21] proteins[22] are widely studied and recently *p*-nitroaniline as solvatochromic dye was attached to dendronized polymers (DPs).[23] However, in these cases, the dye monomers are assembled on the scaffold. Given their limited overlap integral in absorption and fluorescence, the HOMO-FRET rate in these systems is certainly low. For instance, the cyanine dye monomers cou-

pled on DNA (with up to ~30 nm in length) have a transfer efficiency of ~2% in solution.[24] The mechanism of linear helical J-aggregate formation on DNA templates is a sequential process of inserting a co-facial (H-type) dimer into the minor groove of DNA, followed by dislodging the dimers into a higher-order aggregate (H- or J-). Consequently, the groove gets perturbed to facilitate another dimer for binding. In a cooperative fashion, this array of dimers forms an aggregate.[19, 20] It can be postulated that the coupling between adjacent dimers maybe very weak leading to exciton localization across the DNA. Moreover, the presence of J-dimers will adversely localize the exciton on the J-aggregate channel due to the large bandgap of the former.

We thus followed a different approach and anchored J-aggregates of a cyanine dye (Figure 1) already present in solution onto a template. As one-dimensional templates we used dendronized polymers (DPs), which is a class of comb polymers where a linear backbone bears a dendritic (*i.e.* regularly and repeatedly branched) side chain.[25, 26] An important parameter for the description of these polymers is the dendritic generation number *g*, which corresponds to the number of branching points between a peripheral group and the focal point by which the dendritic side groups are attached to their common core. By virtue of the very compact structure of the dendritic side chains, diameter becomes a parameter which can be varied in discrete steps by altering *g*, thereby influencing *e.g.* the overall stiffness of the polymers[27, 28] and creating a separation between "interior" and "exterior" at sufficiently high *g*.[23, 29] Another feature of interest is the large number of peripheral groups, which permits the facile modification of peripheral functionality. The DPs used in this publication feature a methacrylate-based backbone and twofold-branching dendritic side chains bearing peripheral amines (in the form of their trifluoroacetate salts, see Figure 1). In solution, the degree of protonation of primary and tertiary amnes can be controlled via the pH. That also implies an easy control of the charge density of the DP. Furthermore, the DPs are water soluble and are adhering strongly to oxide surfaces.[30] These properties have previously been utilized to immobilize DP-enzyme conjugates on a variety of solid supports like mica, silica, gold and highly ordered pyrolytic graphite (HOPG).[31-34]

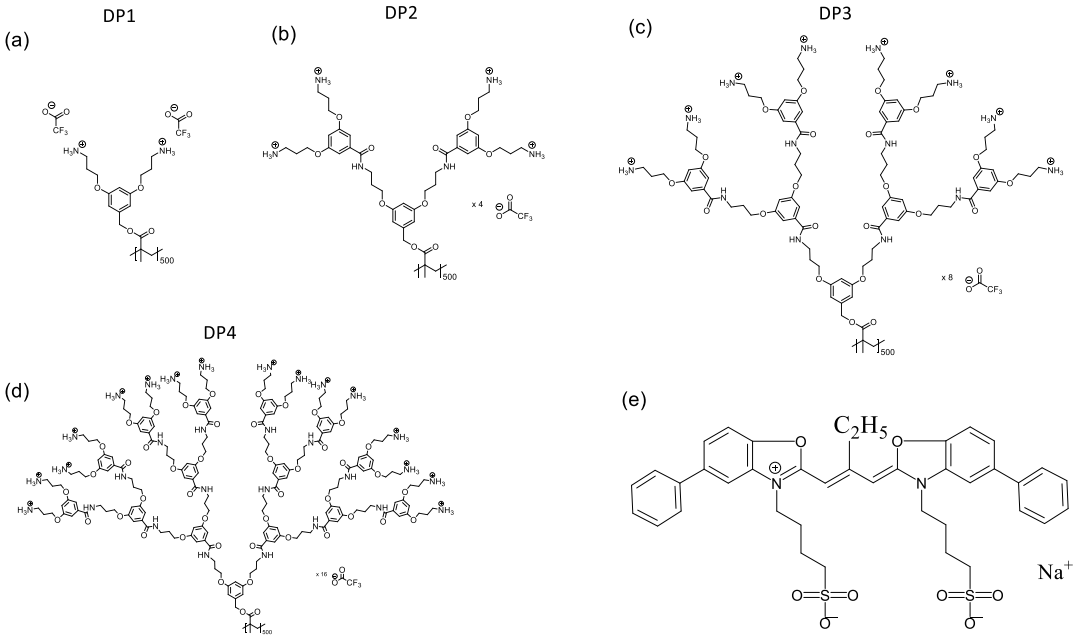

Figure 1. Chemical structures of the DPs featured in this publication (DP1, DP2, DP3 and DP4) as shown in (a-d) and the cyanine dye **J560** used for J-aggregate formation (e).

The interaction between DPs and J-aggregates is mainly of electrostatic nature, the positively charged protonated amine groups of the DPs can bond to the negatively charged sulfonate groups of the J-aggregates. In a first approach, we adsorbed the J-aggregates onto a monolayer of DPs formed on a substrate. However, we showed that it is a real challenge to adsorb a continuous J-aggregate layer on DPs. The aggregates assembled in irregular crystals and largely loose the sharpness of their solution absorption peak and low presence of monomers. Differently, absorbing J-aggregates onto the DPs in solution first and then anchoring the composite onto the substrate led to spectroscopically well-defined aggregates. We proved that the aggregates indeed anchor to the DPs in solution by following their conformational changes with Small Angle X-ray Scattering (SAXS). Finally, we have explored a layer-by-layer approach to anchor the J-aggregate nanowires on glass substrates.

2. Results and Discussion

2.1 Dye aggregation in solution

The specific dye (**J560,** for molecular structure see Figure 1) was chosen for this investigation as it favors aggregation under acidic conditions, where amine groups in the DPs are also protonated. First, we will discuss J-aggregate formation in solution. We show that the process of J-aggregate self-assembly of the dye **J560** is a complex but hierarchical process influenced by solvent polarity, ionic strength, and the dye content. The **J560** dye was dissolved in methanol (c = 0.2 mM), water (c = 0.2 mM) and 100 mM acetate buffer (c = 0.04 mM). In methanol, only the monomer (M) form of the dye was observed with peak absorption at 504 nm (Figure 2). Even though the presence of sulphonate groups in the dye (see Figure 1) procure water solubility, water induces J-aggregation (marked J) and H-type dimers (D) visible as red– and blue shifted peaks in the UV-vis spectrum next to remnant monomers. Dye in 100 mM acetate buffer led to complete formation of J-aggregates (peak absorption at 560 nm) with a minimum amount of remnant monomers. Modifying the ionic strength of the buffer solution straddles the equilibrium between dimer (D) and J-aggregate (data not shown here). The molar extinction coefficient and full-width at half-maximum (FWHM) of the J-aggregate in solution was 2.194×10^5 cm^{-1} and 17.1 nm respectively. J-aggregates formed in acetate buffer have a higher quality than J-aggregates formed in water.

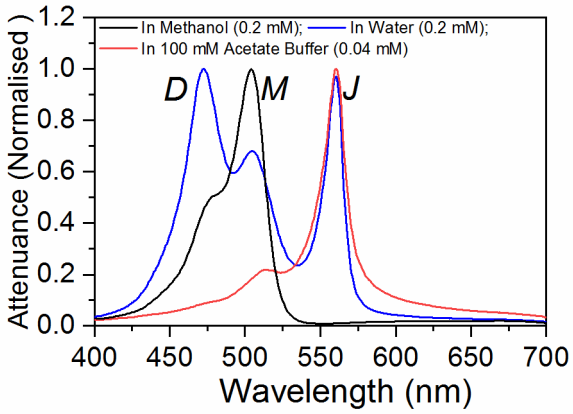

Figure 2. Attenuance (normalized) for **J560** dye dissolved in methanol, water and 100 mM acetate buffer.

2.2 Conformation of different generation DPs on glass substrates and anchoring J-aggregates

In a first step, glass substrates were functionalized with different generation DPs by immersing them in a DP solution (~100 mg L^{-1} in 100 mM acetate buffer) for 30 min, followed by rinsing with acetate buffer and water. Under these conditions the polymer chains are highly positively charged and the DPs of 4th generation (DP4) form a densely packed monolayer on glass or mica substrates (AFM image Figure 3d). The DPs showed rod-like structures, with rather elongated chains (compared to less dense packed polymers at the same ionic strength) and an almost equidistant spacing between the individual polymers.[35] The maximum line charge density of this polymer has been reported to be 60 nm^{-1},[35] speaking for a high charge-density of the DP4 monolayer. For more information on the optimization conditions, please refer the Supporting Information, Section S1, Figures S1 to S5. Under the same conditions, films of DP3 formed a similar monolayer, but on top of that excess DPs collapsed into toroid shaped condensates (Figure 3c). The exact origin of this condensation is not clear, and also not subject of this publication. But, the dendronized polymers of lower generation have a much lower line charge density (30 nm^{-1} and 60 nm^{-1} for DP3 and DP4, respectively)[35] and the similarity to DNA toroids, especially the monodispersity of the condensates, speaks for a similar formation mechanism. Ubbink and Odijk calculated the stability conditions for DNA hexagonally packed within a toroid.[36] We propose that the glass surface is decorated with a higher charge density than a DP3 monolayer could possibly be charged with, leading to the assembly of toroids on the DP3 monolayer. The trend for ring structure formation continued for DP2 and DP1 (Figure 3 a and b) which have even lower line charge densities (7.5 and 15 nm^{-1} for DP1 and DP2, respectively).[35] Toroidal DNA condensates have been identified as a method by nature to pack genomes at high density.[37] The conformations were verified for their homogeneity across the sample under AFM at several spots (data not shown here).[36, 37] In the next step, we will discuss the influence of these DP conformations towards J-aggregation.

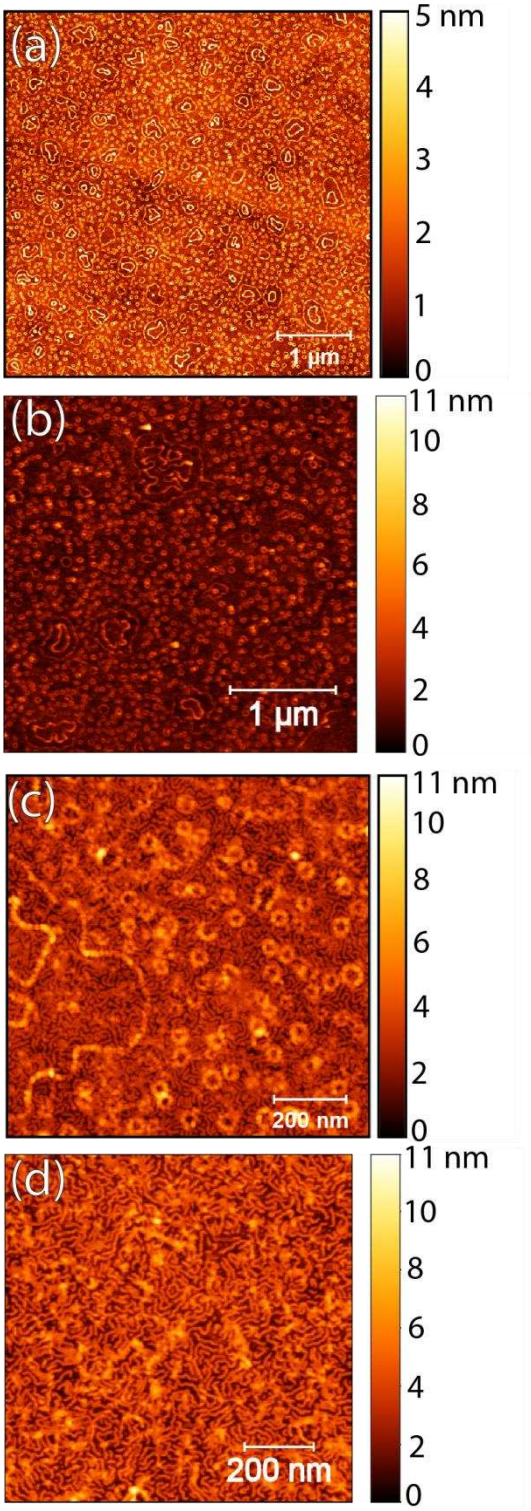

Figure 3. Conformation of different generations of DP – (a) DP1, (b) DP2, (c) DP3 and (d) DP4 on glass substrates.

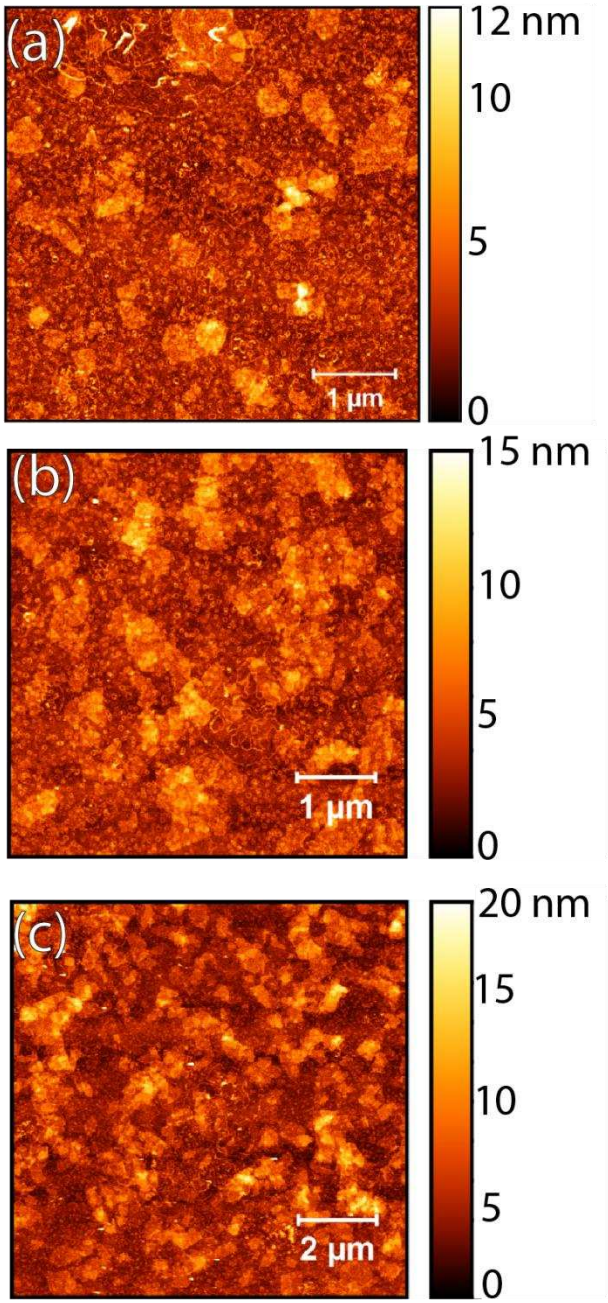

Figure 4. Topography of J-aggregates deposited on DP2 functionalized glass from (a) 0.2 mM, (b) 0.6 mM and (c) 2 mM solutions of J560 in 100 mM acetate buffer.

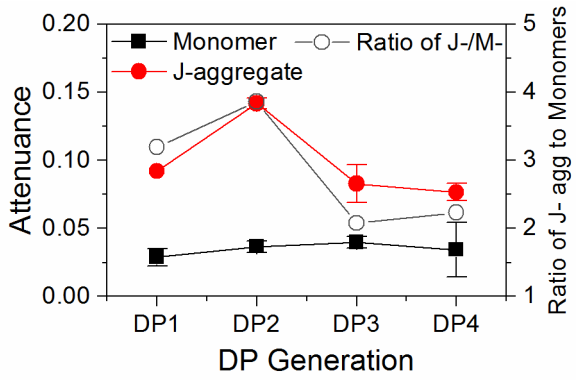

Figure 5. Attenuance of monomers and J-aggregates deposited on DP functionalized glass substrates.

Glass substrates uniformly covered with DP films were immersed in c = 0.6 mM dye solution in 100 mM acetate buffer and left overnight in a shaker. Under these conditions the dye is present in the form of J-aggregates (see section 2.1). Then, the substrates were rinsed following the same procedure as described for DP monolayer formation. With a pH of the acetate buffer between ~3.5 and 4, we expect both the primary and tertiary amines of the DPs to be protonated. These protonated amines interact with the sulphonate groups of the dye to anchor the J-aggregates at the amine sites of the DPs deposited on the glass substrates. The attenuance of the J-aggregate films are shown in Figure S6, Supporting Information. Compared to the solution spectra, the spectral peaks showed significant broadening and contributions from monomers and dimers. AFM images of the aggregates adsorbed from solution are shown in Figures 4 and S7. The aggregates adsorbed from solution crystallized into larger objects following a Volmer-Weber growth model and did not form conformal coatings on the DPs.[17] This process was independent of DP generation and dye solution concentration. The crystal morphology is typical for J-aggregates deposited onto functionalised substrates.[17, 38] The attenuance spectra of J-aggregates on DPs of different generation can be analysed further. Attenuance intensity of monomer, J-aggregate and the ratio between J-aggregate and monomer are shown in Figure 5. No adsorption of J-aggregates on glass substrates was observed in the absence of DP layer. It can be clearly noted that the J-aggregate peak intensity was maximized for DP2. The ratio of J-aggregate to monomer absorption is also shown to verify that the normalized

data are still following the same trend. This observation suggests a correlation between the conformation of the DP and the aggregation behavior. The dye formed better (i.e high *J*-/*M*- ratio) J-aggregates on ring-like DPs (DP1 and DP2) than on the rod-like DPs (DP3 and DP4). It can also be seen that the dimer (*D*) absorption started to increase with DP3 and DP4. Effectively, the J-aggregate films on DP3 and DP4 showed a higher dimer and monomer fraction than the starting solution. That is different from the cooperative mechanism of dimers forming a J-aggregate on DNA as reported elsewhere,[19, 20] where the dimers act as nucleation site for further J-aggregate growth.

We postulate here and we confirmed with small-angle x-ray scattering studies in the following discussion, that the density of dendrons packed in a DP increases with DP order. Only monomers and dimers but not larger aggregates can access the interior of DPs where they bind to the protonated amines. Following the previous arguments, this effect was more pronounced for DPs of higher generation. Indeed, when using a solution with higher dye concentration, resulting in larger aggregates (c = 2 mM dye in 100 mM acetate buffer), a further decrease in J-aggregate absorption was observed (Figure S6 (b) and (d)). Furthermore, in our case, the DPs were strongly adsorbed on the glass surface which limits their conformational flexibility when the dyes anchor on the surface, similar to DNAs.[19, 20] Conclusively, when the polymers are pre-adsorbed on glass (solid) substrates, J-aggregation is more prominent on low generation DPs than higher generation DPs. Here no tubular morphology was observed.

2.3 Complexation of J-aggregate and dendronized polymers in solution studied by SAXS

To relax the conformational constraint of the thin films imposed on higher order DPs upon adsorbing onto a substrate, we moved towards complexing DPs and J-aggregates in solution. Both, DP2 and DP4 in 5 wt% acetate buffer solutions were prepared and different amounts of J-aggregate solution were added to maintain 0.2 mM, 0.6 mM and 2 mM dye concentration (See Supporting Information, Figure S8). The solution was stirred overnight and introduced into quartz capillaries for the X-ray diffraction measurement.

The solution incorporating second generation of dendronized polymers (DP2) was characterized with increasing amounts of dye molecules added to the sample. The SAXS scattered intensities as a function of the scattering vector magnitude, q, for those samples and the pure dye sample at 2 mM concentration are presented in Figure 6 (a) together with their corresponding simulated curves. Fits of the corresponding pair-distance distribution functions, p(r)'s, are shown in Figure 6 (b), as obtained from indirect Fourier transformation (IFT) analysis of scattering data and helps in the interpretation of the systems' structural behavior in real space. The p(r) from the pure polymer represents an asymmetric behavior; a sharp peak appears at around 2.9 nm while a (semi-)linear decay shows up at higher dimensions, reaching zero at around 22 nm. Such p(r) behavior typically represents elongated particles (cylindrical structures) with maximum dimension (D_L) of about 22 nm. To obtain further information about the cross section of the cylindrical structures, before and after loading with dye molecules, the scattering from the cylinder cross-section, $I_{cs}(q)$ was separated from the cylinder length (proportional to q^{-1}) via $I_{cs}(q) = I(q) \times q$. The resulting $I_{cs}(q)$ curves are presented in Figure 6 (c). These corresponding p(r) functions demonstrate the spatially averaged convolution square of electron density fluctuations within the cross section of polymer chains. The cross-sectional p(r) for the pure polymer shows a bimodal distribution with a maximum cross-section dimension (D_{cs}) of 5.3 nm.

A similar behavior has been observed for polymer samples loaded with 0.2 and 0.6 mM of dye; the p(r) presented in Figure 6(d) shows an increase in D_L up to 33 nm. The p(r) of the cross-section also demonstrates a slight increase after adsorption of dye molecules on the polymer chains (from D_{cs} =5.3 nm for pure polymer to 6.6 nm in presence of 0.6 mM of dye). Interestingly, the bimodal feature in p(r) is suppressed and a uniform electron density distribution across the polymer could be identified. It can be concluded that adsorption of dye molecules occurs at every radial distances from the center of the polymer (both at the interior as well as the surface of polymer chain).

At very high concentrations of dye (2 mM), the scattering patterns resemble the ones obtained from pure dye aggregates, only with extension to higher D_{max} (see a broad distribution peak

at around 12 nm in Figure 6 (b), blue and gray curves). This indicates that at such high concentrations of dye, the polymer is saturated and cannot uptake the dye molecules any further and hence a considerable amount of dye aggregates form in the medium. It can be noted that the trend observed in attenuance for the J-aggregates deposited on DP2 pre-functionalized substrates shown in Figure S6 (b) goes in hand with the SAXS measurement in solution: at the optimized dye concentration of 0.6 mM, the J-aggregate size is such that it is able to reach both the interiors and exteriors amine functional sites in the DP2. Increasing the dye concentration to 2 mM, drastically increased the J-aggregates size, which inhibited the accessibility to interior amine groups leading to a decrease in adsorption of J-aggregates (Figure S6 (b)).

SAXS measurements on the fourth generation dendronized polymers (DP4) revealed a similar behavior of the dye absorption on polymer chains. First of all, the D_L for DP4 showed similar values as DP2, an increase in D_L for pure polymer from around 23.5 nm to 33.5 nm for polymer after adsorption of 0.6 mM dye could be measured. However, the cross-sectional dimensions were significantly different, D_{cs} = 8.8 nm for pure polymer and D_{cs} = 9.7 for polymer in presence of 0.6 mM dye. Such increased cross-sectional dimensions are in good agreement with our estimations from the molecular structure of the polymer. In addition, similar to what has been observed for DP2, the bimodal feature in cross section p(r) of the DP4 diminished after adsorption of dye, indicating a morphological transformation of the cross-section from a core-shell structure to a homogeneous electron density (Figure 7(d)). Hence, dye molecules appear to distribute across the cross-section of DP4 rather than only at the surface.

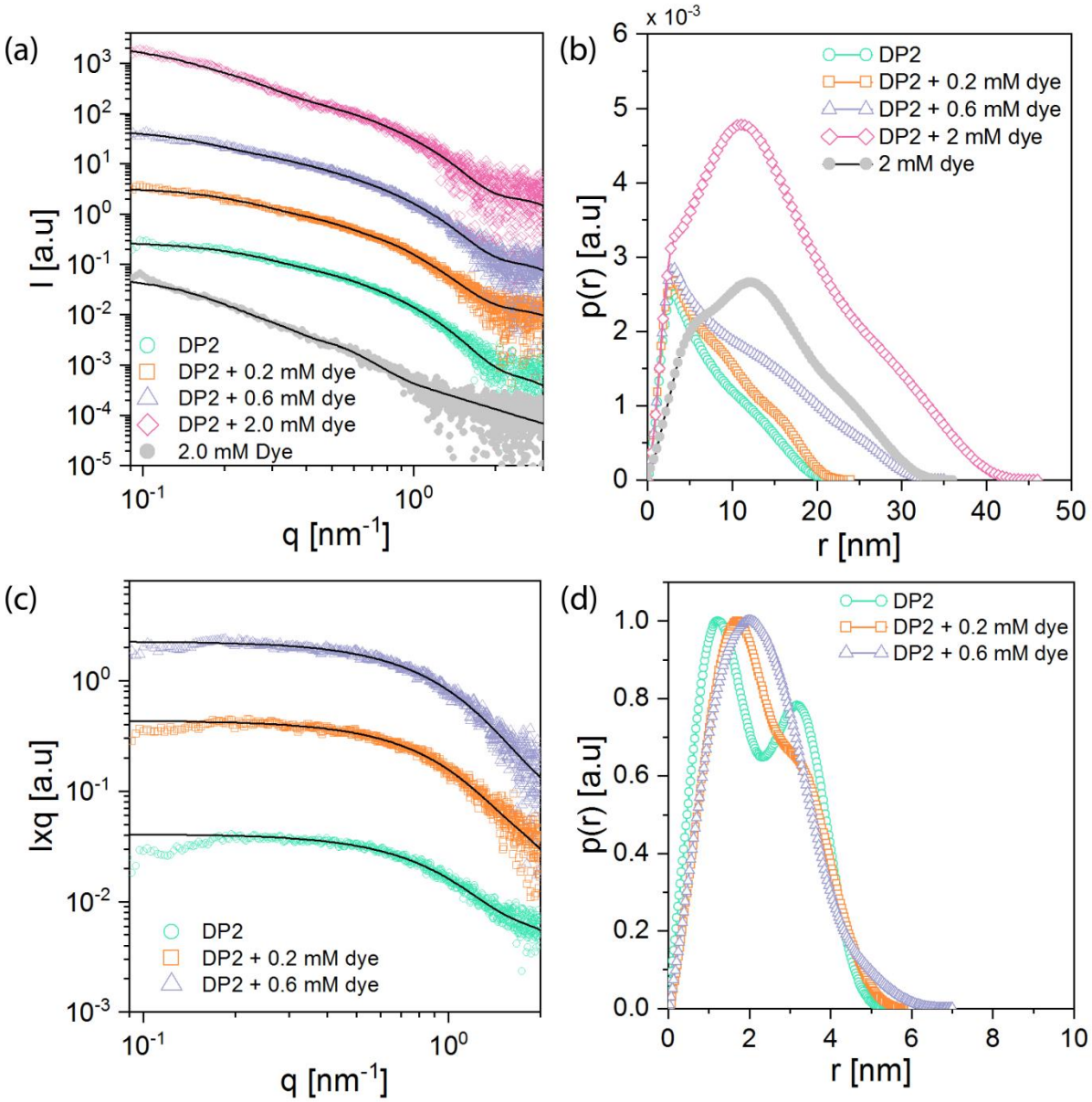

Figure 6. (a) The experimental I(q) profiles of DP2 polymer and the dye (pure and their mixtures) shown in dots and their corresponding theoretical curves (solid lines) calculated from the IFT analysis. For better representation, the curves are shifted vertically. (b) represents the p(r) functions relevant to the theoretical curves shown (a). (c) the I×q versus q curves for DP2 polymer-dye mixtures representing cross-section scattering intensities. These curves analyzed by IFT to obtain detailed cross sectional information. For better representation, the curves are shifted vertically. (d) The resulting p(r) functions for scattering shown in (c).

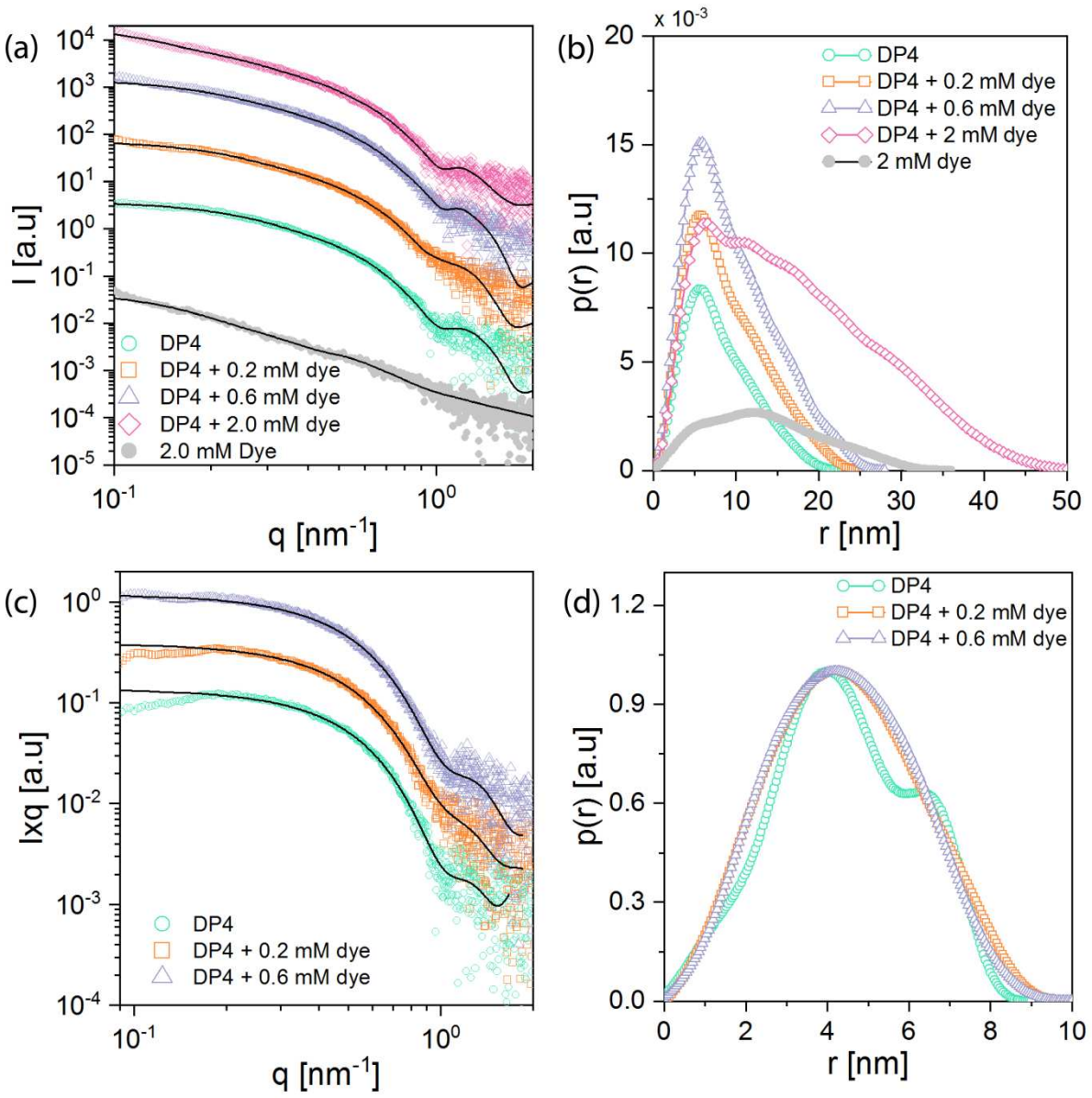

Figure 7. (a) The experimental I(q) profiles of DP4 polymer and the dye (pure and their mixtures) are shown in dots along with their corresponding theoretical curves (solid lines) calculated from the IFT analysis. For better representation, the curves are shifted vertically. (b) represents the p(r) functions relevant to the theoretical curves shown (a). (c) the I×q versus q curves for DP4 polymer-dye mixtures representing cross-section scattering intensities. These curves are analysed by IFT to obtain detailed cross sectional information. For better representation, the curves are shifted vertically. (d) The resulting p(r) function for scattering shown in (c).

Table 1: Maximum elongated dimension (D_L) and maximum cross-section dimension (D_{cs}) for DP2 and DP4 covered with different dye loadings. Inherent to the geometrical limitation to access low q values in the Guinier regime, the dimensions mentioned below are an underestimate, but the trend is still relevant.

Sample details	Maximum elongated dimension (D_L), in nm		Maximum cross-section dimension (D_{cs}), in nm	
	DP2	DP4	DP2	DP4
Pure DP	22	23.5	5.3	8.8
DP + 0.2 mM dye	23	25	5.7	9.7
DP + 0.6 mM dye	33	29	6.6	9.7
DP + 2 mM dye	35	53	NA	NA

2.4 Layer-by-layer anchoring of J-aggregate nanowires

SAXS experiments proved that the dye molecules are homogeneously covering the DP's interior and exterior surfaces for a dye concentration of c = 0.6 mM. Also, the SAXS measurement showed an increase in elongated dimension for both the DP2 and DP4 generation upon addition of dye. We next adsorbed the J-aggregate nanowires onto substrates, with the hope that the J-aggregates maintained their superior solution properties while being easily processed. We have tested a layer-by-layer (LBL) approach to adsorb the nanowires onto a substrate. The J-aggregate/DP nanowires did not adsorb onto glass substrates, but on substrates functionalized with a monolayer of DP. We can conclude that the dye/DP nanowires show a negative excess charge from the dye. The glass substrates were functionalized with monolayers of DP (as shown in Figure 3) and exposed to the J-aggregate/DP nanowire solution. After an immersion time of 24 h, the substrates were rinsed with water and imaged under an AFM. The J-aggregate/DP nanowires adsorbed with low density on the DP2 functionalized surface. They showed an elongated rod-like structure. Already SAXS suggested a stretching of the DP chains upon dye loading, even though a direct comparison is difficult because the substrate has a major influence on the conformation. The morphology differed dramati-

cally from J-aggregates adsorbed onto DP monolayers (Figure 5) and unloaded DPs (Figure 3). It can be noted that the nanowires preferentially adsorb on top of the "isolated" rings, in-line with the earlier interpretation that the potential at the outer DP layer is most positive.

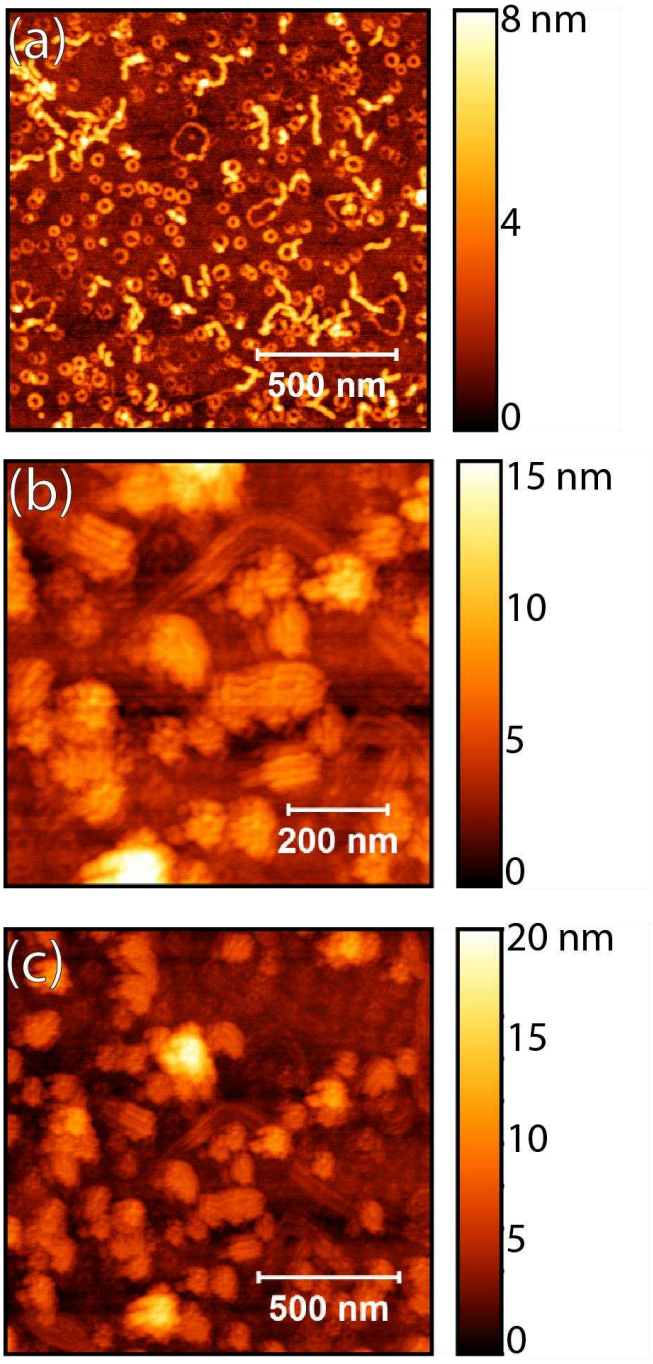

Figure 8. Elongated DP2 (a) and DP4 (b) deposited from complexed DP and J-aggregate solution (*c* = 0.6 mM dye in acetate buffer) on their corresponding DP pre-functionalized glass substrates. For DP4, *super-structures* were observed with local ordering when they are covered with dye molecules as shown in (c).

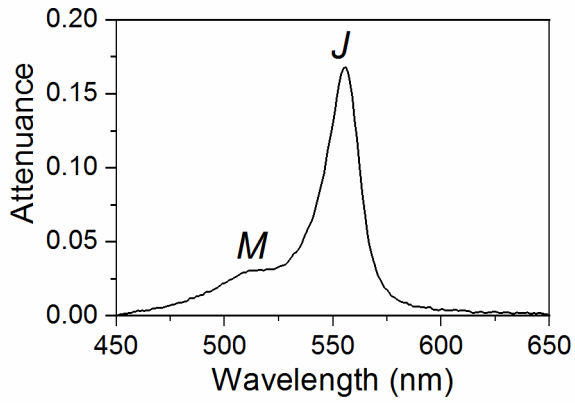

Figure 9. Attenuance for DP4-premixed with dye solution (c = 0.6 mM) and deposited on DP4 functionalised glass substrates.

DP4 coated with dye molecules assembled into long *fibrous bundle-like* structures when deposited on the substrate (Figure 8 a and b). This can be explained by a reduction of electrostatic repulsion between J-aggregate/DP nanowires, the positive charge of the DPs is compensated by the negative charge of the dye aggregates anchoring on the DP surface. These type of nanotubular bundles are also famously present for tubular J-aggregates.[39] Another type of structure– *supercoiling*, is influenced by the DPs interaction with substrates.[40] Also, a block co-polymer coupled to DP is known to generate nanoscale building block materials.[41] In a similar fashion, complexing the cyanine dye J-aggregates with DP4, showed a supercoiling effect, which is reflected in the topography (Figure 8 (c)).

Differently from the aggregates directly assembled onto a substrate (Figures 5 and S8), no crystalline features were observed. Larger J-aggregate crystallites are prone to self-quenching from defects like grain boundaries resulting from the spontaneous self-assembly process. Moreover, static disorder is one of the limiting factors for extended diffusion length in large aggregate crystals. Further information on the "quality" of a J-aggregate can be also extracted from UV-Vis spectroscopy. Absorbance spectra of the J-aggregate/DP nanowires in thin films are shown in Figure 9. It can be noticed that the J- to M- intensity is much higher in J-aggregate/DP nanowires compared to J-aggregates deposited on DPs (Figure S6(d)) for the same dye concentration (c =0.6 mM). Also,

the dimer absorption is negligible when using the solution complexation route (Figure 9) compared to depositing the aggregates on DP functionalised substrates (Figure S6 (d)). This underscores the significance of the conformations of the polymer required towards J-aggregation. In fact, the DP acted as a much better linear template to anchor J-aggregates than conventional DNA assemblies, which are difficult to functionalise with J-aggregates already present in the solution.

Conclusion

We here demonstrated the potential of complexing DPs and J-aggregates in solution as a new method to form coherent tubular aggregates with improved properties in thin film. Critical for the ability of the J-aggregate to anchor to the interior and exterior dendrons of the DP is the dye concentration (size of aggregates) and generation of the DPs. The J-aggregate/DP nanowires can be easily transferred onto a substrate.

This process also allows to disperse J-aggregates into other matrix materials, where they could act as energy transport channels in FRET mode. Moreover, due to the versatility of this growth technique, J-aggregates could be grown on defined pathways which are exciting areas for building electronic devices. Further steps will be to study the role of these tubular aggregates as excitonic channels in excitonic transistors. Specifically, we believe that this method can be extended to study donor-acceptor systems for energy transfer studies and in photovoltaics.

Experimental Section

Dendronized polymers of generation 1 - 4 were synthesized by following solid state peptide synthesis as described elsewhere.[30] Glass substrates were cleaned in acetone, ethanol, Hellmanex soap solution and water (3 times) with 5 min ultrasonication for each step separately. The substrates were dried using a N_2 gas stream and treated with oxygen plasma for 5 min to remove any organic residues. To deposit the DP on glass, the substrates were immersed in a solution of DP dissolved in 100

mM acetate buffer for 30 min and rinsed with acetate buffer followed by rinsing in water and N_2 drying. Cyanine dye (5-Phenyl-2-[2-[[5-phenyl-3-(4-sulfobutyl)-3H-benzoxazol-2-ylidene]-methyl]-but-1-enyl]-3-(4-sulfobutyl)-benzoxazolium hydroxide, inner salt, sodium salt) abbreviated as **J560**, was dissolved in methanol, water and acetate buffer at different concentrations to study the monomer to J-aggregate formation in solution. To achieve DPs covered with J-aggregate assemblies, the dye solution and DP solution were mixed together. The surface topography of the adsorbed layers was studied using atomic force microscopy (Bruker Dimension Icon) with an Antimony-doped Si cantilever (RTESP 300, tip radius of 12 nm, force constant of 40 Nm^{-1}, resonant frequency 300 kHz) procured from Bruker and images were analysed using the Nanoscope software. UV-Visible spectra for J-aggregate were acquired using a Varian Cary 50 UV-Vis spectrophotometer.

The SAXS experiments were performed using a Nanostar SAXS system (Bruker AXS GMBH, Karlsruhe, Germany) equipped with microfocuses X-ray source (Cu K_α radiation) and MONTEL optics providing a point-focused X-ray beam with 0.154 nm wavelength. A VÅNTEC-2000, Xe-based gaseuse avalanche detector capable of photon counting with 0.5 seconds temporal resolution, positioned at sample to detector distances of about 67 cm was used to acquire the scattering patterns. The acquisition time was 2 h. The setup is optimized and aligned to achieve the minimum scattering vector modulus of 0.1 nm^{-1}. All the experiments were performed at room temperature.

The DP samples and its mixtures with dye solution were transferred into disposable quartz capillaries of 1.5 mm in outer diameter (Hilgenberg GmbH, Malsfeld, Germany). The capillaries were sealed prior mounting in the sample chamber. The scattering patterns from empty capillary and acetate buffer filled ones were also recorded for background subtraction.

Acknowledgement

The authors gratefully acknowledge funding from the Swiss National Science Foundation grant number: 200021-157135 to conduct this research work. We acknowledge the Scanning Probe Microscopy user laboratory at Empa for providing access to the instrument.

References

1. E. Romero, V. I. Novoderezhkin and R. van Grondelle, *Nature*, 2017, **543**, 355.
2. T. Mirkovic, E. E. Ostroumov, J. M. Anna, R. van Grondelle, Govindjee and G. D. Scholes, *Chemical Reviews*, 2016, DOI: 10.1021/acs.chemrev.6b00002.
3. D. Möbius, *Advanced Materials*, 1995, **7**, 437-444.
4. D. M. Eisele, J. Knoester, S. Kirstein, J. P. Rabe and D. A. Vanden Bout, *Nature Nanotechnology*, 2009, **4**, 658.
5. B. J. Walker, V. Bulović and M. G. Bawendi, *Nano Letters*, 2010, **10**, 3995-3999.
6. C. Wang and E. A. Weiss, *Nano Letters*, 2017, **17**, 5666-5671.
7. D. M. Eisele, J. Knoester, S. Kirstein, J. P. Rabe and D. A. Vanden Bout, *Nature Nanotechnology*, 2009, **4**, 658-663.
8. K. A. Clark, E. L. Krueger and D. A. Vanden Bout, *The Journal of Physical Chemistry Letters*, 2014, **5**, 2274-2282.
9. H. von Berlepsch, C. Böttcher, A. Ouart, C. Burger, S. Dähne and S. Kirstein, *The Journal of Physical Chemistry B*, 2000, **104**, 5255-5262.
10. E. Lang, A. Sorokin, M. Drechsler, Y. V. Malyukin and J. Köhler, *Nano Letters*, 2005, **5**, 2635-2640.
11. N. Kameta, K. Ishikawa, M. Masuda, M. Asakawa and T. Shimizu, *Chemistry of Materials*, 2012, **24**, 209-214.
12. D. M. Eisele, C. W. Cone, E. A. Bloemsma, S. M. Vlaming, C. G. F. van der Kwaak, R. J. Silbey, M. G. Bawendi, J. Knoester, J. P. Rabe and D. A. Vanden Bout, *Nature Chemistry*, 2012, **4**, 655-662.
13. K. A. Clark, C. W. Cone and D. A. Vanden Bout, *The Journal of Physical Chemistry C*, 2013, **117**, 26473-26481.
14. J. Yuen-Zhou, D. H. Arias, D. M. Eisele, C. P. Steiner, J. J. Krich, M. G. Bawendi, K. A. Nelson and A. Aspuru-Guzik, *ACS Nano*, 2014, **8**, 5527-5534.
15. D. M. Eisele, D. H. Arias, X. Fu, E. A. Bloemsma, C. P. Steiner, R. A. Jensen, P. Rebentrost, H. Eisele, A. Tokmakoff and S. Lloyd, *Proceedings of the National Academy of Sciences*, 2014, **111**, E3367-E3375.
16. J. L. Banal, T. Kondo, R. Veneziano, M. Bathe and G. S. Schlau-Cohen, *The Journal of Physical Chemistry Letters*, 2017, **8**, 5827-5833.
17. S. B. Anantharaman, T. Stöferle, F. Nüesch, R. Mahrt and J. Heier, *(Submitted)*, 2018.
18. H. v. Berlepsch and C. Böttcher, *Physical Chemistry Chemical Physics*, 2018, **20**, 18969-18977.
19. M. Wang, G. L. Silva and B. A. Armitage, *Journal of the American Chemical Society*, 2000, **122**, 9977-9986.
20. K. C. Hannah and B. A. Armitage, *Accounts of Chemical Research*, 2004, **37**, 845-853.
21. C. M. Soto, A. S. Blum, G. J. Vora, N. Lebedev, C. E. Meador, A. P. Won, A. Chatterji, J. E. Johnson and B. R. Ratna, *Journal of the American Chemical Society*, 2006, **128**, 5184-5189.
22. K. D. Volkova, V. B. Kovalska, A. O. Balanda, R. J. Vermeij, V. Subramaniam, Y. L. Slominskii and S. M. Yarmoluk, *Journal of Biochemical and Biophysical Methods*, 2007, **70**, 727-733.
23. C. Gstrein, B. Zhang, M. A. Abdel-Rahman, O. Bertran, C. Alemán, G. Wegner and A. D. Schlüter, *Chemical Science*, 2016, **7**, 4644-4652.

24. S. A. Díaz, S. M. Oliver, D. A. Hastman, I. L. Medintz and P. M. Vora, *The Journal of Physical Chemistry Letters*, 2018, **9**, 3654-3659.
25. H. Frauenrath, *Progress in Polymer Science*, 2005, **30**, 325-384.
26. A. D. Schlüter, A. Halperin, M. Kröger, D. Vlassopoulos, G. Wegner and B. Zhang, *ACS Macro Letters*, 2014, **3**, 991-998.
27. Y. Guo, J. D. van Beek, B. Zhang, M. Colussi, P. Walde, A. Zhang, M. Kröger, A. Halperin and A. Dieter Schlüter, *Journal of the American Chemical Society*, 2009, **131**, 11841-11854.
28. B. Zhang, R. Wepf, M. Kröger, A. Halperin and A. D. Schlüter, *Macromolecules*, 2011, **44**, 6785-6792.
29. C. Gstrein, P. Walde, A. D. Schlüter and T. Nauser, *Photochemical & Photobiological Sciences*, 2016, **15**, 964-968.
30. B. Zhang, R. Wepf, K. Fischer, M. Schmidt, S. Besse, P. Lindner, B. T. King, R. Sigel, P. Schurtenberger, Y. Talmon, Y. Ding, M. Kröger, A. Halperin and A. D. Schlüter, *Angewandte Chemie International Edition*, 2011, **50**, 737-740.
31. F. Sara, B. T. E., Z. Baozhong, S. A. Dieter and W. Peter, *Macromolecular Bioscience*, 2011, **11**, 1052-1067.
32. F. Sara, K. Phillip, L. Dario, S. A. Dieter, D. P. S. and W. Peter, *ChemPlusChem*, 2012, **77**, 98-101.
33. A. Küchler, J. Adamcik, R. Mezzenga, A. D. Schlüter and P. Walde, *RSC Advances*, 2015, **5**, 44530-44544.
34. A. Küchler, D. Messmer, A. D. Schlüter and P. Walde, in *Methods in Enzymology*, ed. C. V. Kumar, Academic Press, 2017, vol. 590, pp. 445-474.
35. L. Grebikova, S. Kozhuharov, P. Maroni, A. Mikhaylov, G. Dietler, A. D. Schlüter, M. Ullner and M. Borkovec, *Nanoscale*, 2016, **8**, 13498-13506.
36. J. Ubbink and T. Odijk, *Biophysical Journal*, 1995, **68**, 54-61.
37. C. C. Conwell, I. D. Vilfan and N. V. Hud, *Proceedings of the National Academy of Sciences*, 2003, **100**, 9296-9301.
38. M. S. Bradley, J. R. Tischler and V. Bulović, *Advanced Materials*, 2005, **17**, 1881-1886.
39. K. A. Clark, E. L. Krueger and D. A. Vanden Bout, *The Journal of Physical Chemistry C*, 2014, **118**, 24325-24334.
40. V. Percec, C. H. Ahn and B. Barboiu, *Journal of the American Chemical Society*, 1997, **119**, 12978-12979.
41. C. Li, A. D. Schluüter, A. Zhang and R. Mezzenga, *Advanced Materials*, 2008, **20**, 4530-4534.